Two-Dimensional Modeling of Electroremediation

Richard A. Jacobs and Ronald F. Probstein
Dept. of Mechanical Engineering, Massachusetts Institute of Technology, Cambridge, MA 02139

A mathematical model and numerical code for the simulation of contaminant removal from soils by electric fields are applied in two dimensions. The model describes the coupled transport of mass and charge, and the chemical speciation of a multicomponent system subjected to an electric field. Transport mechanisms included are electroosmosis, pressure-driven convection, electromigration, and diffusion. The model can also describe complexation, dissolution and precipitation reactions, surface complexation and sorption processes, and electrochemical reactions. Chemical and sorption equilibria are assumed. Transport equations used are based on quantities conserved throughout chemical reactions so that only the time scales of transport processes need to be resolved. The model is used to simulate the removal of phenol from kaolin clay for which experiments are presented. The successful explanation of the experimental observations confirms the theoretical bases of the model.

Introduction

The removal of contaminants from soil by applying a dc voltage difference across electrode pairs emplaced in the soil has attracted considerable attention due to its potential to achieve safe and cost-effective *in-situ* remediation of hazardous waste sites. The technique relies mainly on the electrokinetic phenomenon of electroosmosis and on electromigration to drive the contaminants contained in the pore liquid toward predefined electrodes for collection.

Electroosmosis is due to the force generated by the applied electric field on a thin layer of charged fluid in the pore liquid that forms adjacent to charged soil particles. This layer, known as the Debye sheath or double layer, results from the repulsion of coions and attraction of counterions by the pore wall. The electric-field-generated force causes the fluid in the double layer to move, which in turn, sets the bulk liquid in motion by viscous interactions (Probstein, 1994). Electroosmosis generally will dominate over pressure-driven convection in low permeability soils, provided they have a finite charge.

Electromigration originates from the electric force exerted on ionic species, as a result of the applied voltage gradient. The migration velocity is proportional to the product of the species ionic charge and the local electric field. In cases where a significant fraction of the contaminant is in charged form (dissociated acids and bases or metal ions and complexes), electromigration is likely to dominate over other transport mechanisms. Electromigration has been used in both the laboratory and the field to remove metals from soils (Runnells and Larson, 1986; Hamed et al., 1991; Lageman, 1993; Hicks and Tondorf, 1994).

Other common physicochemical phenomena that are also present are: species diffusion in solution; chemical reactions in the bulk liquid; precipitation or dissolution of solid species; interactions with the soil such as adsorption, ion exchange and surface complexation; and electrochemical reactions.

The complex interactions between all these phenomena make it difficult to extrapolate the response of a system from previous experimental observations or practical experience. Significant efforts have therefore been devoted to the development of a mathematical model of the electroremediation process.

The first rational theoretical model was introduced by Shapiro et al., 1989. These authors presented a one-dimensional (1-D) model of the process and successfully applied it to simulate the removal of phenol and acetic acid from kaolin clay. Included were dissociation reactions, electrochemical reactions, and transport due to electroosmosis, electromigration, and diffusion. The basic formulation was later extended to include linear adsorption isotherms and the numerical results compared with additional experiments in Shapiro and Probstein (1993).

Recently, the 1-D model was generalized and a new numerical code was developed to speed up the calculation and

Correspondence concerning this article should be addressed to R. F. Probstein.
Present address of R. A. Jacobs: Maraven S. A. (PDVSA), Div. de Operaciones de Producciòn, P. O. Box 173, Lagunillas, 4016A, Zulia, Venezuela.

to handle more complex chemical systems including arbitrary adsorption isotherms, complexation, and dissolution and precipitation reactions (Jacobs et al., 1994). The generalized approach was applied to simulate the removal of zinc from kaolin clay and produced very good agreement with experimental data.

Another 1-D simulation has been presented by Acar and Alshawabkeh (1994). They calculated the transport of hydrogen ions in a salt solution under constant current conditions. This calculation, however, also assumed constant potential difference and uniform electric field, neglected electroneutrality, and ignored the effect of other ions in solution, so that it is expected to have limited applicability.

While the 1-D model provides useful information about the response of a system, multidimensional systems have additional degrees of freedom that change the solution in ways not easily extrapolated from 1-D results. For example, in one space dimension, the current density is uniform and the electric field varies spatially only with changes in the electrical conductivity and in the concentration gradients. In two and three dimensions, on the other hand, the current density varies with the geometry of the electrode array. As a result, a system with the same chemical speciation may behave differently depending on the number of space dimensions considered in the problem. In order to address this multidimensional effect, a computer model has been developed to simulate the electroremediation process in 2-D geometries. The results from this model can be applied to 3-D systems in which the distance between electrodes is small compared to their length, and there is no significant variation of the material properties with depth.

The code developed computes the time evolution of several state variables (including the spatial distributions of the electrostatic potential and pressure, the current density, and all species velocities and concentrations) in a multielectrode, multicomponent system of arbitrary shape subject to an electric field (Figure 1).

The computer model not only allows the prediction of the system response under specific conditions, but also helps in achieving an understanding of the fundamental phenomenological behavior, as well as speeding up the design of field applications by showing the effect of varying key process parameters on the overall level and rate of contaminant removal. This article presents the most important aspects of the model and its numerical implementation together with the key findings derived from comparison of the numerical results with experiment.

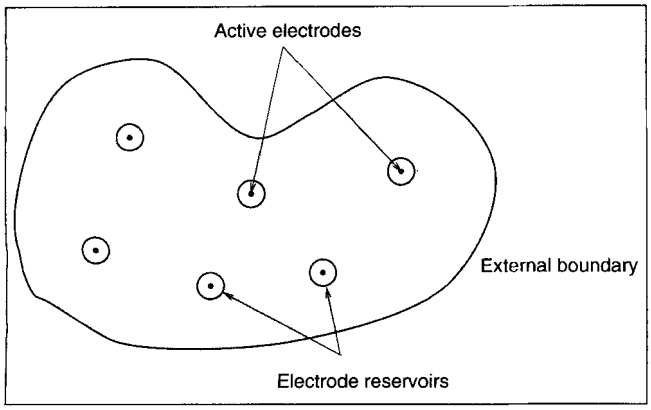

Figure 1. 2-D multielectrode system.

Mathematical Model

Transport mechanisms

The contribution of each transport mechanism to the species flux is derived from the corresponding phenomenological relationship (Probstein, 1994) and extended to an isotropic porous medium using a capillary model.

The bulk liquid velocity $\boldsymbol{u}_c$ in m/s is described as the sum of the contributions due to electroosmosis $\boldsymbol{u}_{eo}$ in m/s and due to any pressure gradient $\boldsymbol{u}_h$ in m/s. The electroosmotic velocity is calculated from the Helmholtz-Smoluchowski relation

$$\boldsymbol{u}_{eo} = \frac{\epsilon\zeta}{\tau^2\mu}\nabla\phi \equiv k_e\nabla\phi \tag{1}$$

where $\boldsymbol{u}_{eo}$ is the interstitial velocity due to electroosmosis in m/s, ϵ the permittivity of the pore liquid in F/m, ζ the zeta potential of the soil in V, τ a nondimensional tortuosity factor that accounts for a nonuniform capillary path and is a number of the order of but greater than 1, μ the viscosity of the pore liquid in Pa·s, ϕ the electrostatic potential in V, and k_e in $m^2/(V\cdot s)$ an effective electroosmotic permeability coefficient used for convenience in the numerical formulation of the model.

The pressure gradient contribution is calculated from Darcy's law

$$\boldsymbol{u}_h = -\frac{k_h}{n\mu}\nabla p \equiv k'_h\nabla p \tag{2}$$

where $\boldsymbol{u}_h$ is the interstitial velocity in m/s resulting from a pressure gradient, k_h the hydraulic permeability of the medium in m^2, n the porosity, and p the pressure in Pa. Again, an effective permeability coefficient k'_h in $m^2/(Pa\cdot s)$ is defined for convenience.

For species i, the electromigration velocity $\boldsymbol{u}_{ei}$ in m/s is given by

$$\boldsymbol{u}_{ei} = -\upsilon_i z_i F\frac{\nabla\phi}{\tau^2} \equiv k_{ei}\nabla\phi \tag{3}$$

where the migration velocity is relative to the pore liquid, υ_i is the mobility, defined as the velocity resulting from a unit force per mole , z_i the charge number, F Faraday's constant, and k_{ei} an effective mobility coefficient in $m^2/(V\cdot s)$.

Finally, the contribution of diffusion to the species flux for dilute solutions is given by Fick's law

$$\boldsymbol{j}_i^d = -\frac{D_i}{\tau^2}\nabla C_i \tag{4}$$

where $\boldsymbol{j}_i^d$ is the molar flux due to diffusion in $mol/(m^2\cdot s)$, C_i the molar concentration of species i in the pore liquid in mol/m^3, and D_i the diffusion coefficient in m^2/s.

Superposing the different mass-transfer mechanisms, the total flux of an individual species is given by

$$j_i = (u_{eo} + u_h + u_{ei})C_i - \frac{D_i}{\tau^2}\nabla C_i \tag{5}$$

or in terms of the gradients of pressure, electrostatic potential, and concentrations by

$$j_i = [(k_e + k_{ei})\nabla\phi + k_h\nabla p]C_i - \frac{D_i}{\tau^2}\nabla C_i \tag{6}$$

where j_i is the molar flux of species i per unit interstitial area in mol/(m^2·s). The coefficients k_e, k_{ei}, k_h, and D_i/τ^2 may vary in space and time.

Equations of change

The equations of change are derived by applying conservation of mass in a control volume of the porous medium which contains both the liquid and solid phases. Neglecting transport of adsorbed species, applying Gauss's divergence theorem, and taking the limit of an infinitesimal control volume leads to

$$\frac{\partial nC_i}{\partial t} + \nabla\cdot nj_i = n(R_i + R_i^a) \quad \text{and} \quad \frac{\partial nC_i^a}{\partial t} = -nR_i^a \tag{7}$$

Here, R_i and R_i^a in mol/(m^3·s) are, respectively, the net volumetric rates of production of chemical species i due to chemical reactions and sorption processes, and C_i^a in mol/m^3 is the molar concentration of species i in the adsorbed phase, all referred to the volume of liquid. The smallest length scale for which Eqs. 7 are applied is large compared with the pore dimensions, so that the species flux can be represented by a continuous function.

Adding the equations for the liquid and solid phases in Eq. 7 gives

$$\frac{\partial n(C_i + C_i^a)}{\partial t} + \nabla\cdot nj_i = nR_i \tag{8}$$

which for a medium of uniform porosity simplifies to the form used in this work

$$\frac{\partial (C_i + C_i^a)}{\partial t} + \nabla\cdot j_i = R_i \tag{9}$$

A similar formulation of the process has been used by Alshawabkeh and Acar (1992). Their formulation, however, is restricted to linear adsorption isotherms.

Numerically integrating the transport equations (Eq. 9) is extremely difficult because the chemical reactions are, in general, several orders of magnitude faster than the transport processes. This is illustrated in Table 1, which shows the characteristic time scales for the main processes of interest in the present problem.

The obstacle of numerically stiff differential equations is overcome by rewriting the transport equations in terms of quantities which are conserved throughout the chemical reactions. This results in transport equations with no generation terms. Based on the conservation principle employed, the conserved quantities T_k can be defined in a number of ways.

Table 1. Characteristic Time Scales

Transport Processes*	Chemical Processes**
Electromigration, 10^2 s	Proton transfer to H_2O, 10^{-12} s
Electroosmosis, 10^4 s	Dissociation of strong acid, 10^{-8} s
Diffusion, 10^5 s	Dissocation of weak acid, 10^{-6} s
	Inorganic complexation, 10^{-6}–10^{-2} s
	Adsorption/Ion exchange, 10^1–10^4 s
	Dissolution/precipitation, 10^2–10^7 s

*Based on a length scale of 0.01 m.
**Adapted from Morel and Hering (1993).

For example, using conservation of elemental mass, T_k can be defined as the total mass of each element; or using conservation of charge, one of the T_k can be the total charge. A suitable set of conserved quantities can also be defined from consideration of the stoichiometry of the chemical equations (Morel and Hering, 1993). In any case, the set of conservation relations will have the form

$$T_k = \sum_{i=1}^{N} \alpha_{ik}(C_i + C_i^a), \quad \forall\, k = 1,\cdots, M \tag{10}$$

where α_{ik} expresses the contribution of each species i to the conserved quantity k, N is the number of species, and M is the number of conserved quantities in the system.

The approach can be illustrated using conservation of elemental mass. The total amount of each element present in the system can be determined using Eq. 10, where α_{ik} is the subscript to element k in the molecular formula of species i, N is the number of species, and M is the number of elements that occur independently in the system. That is, M is the rank of the formula matrix whose entries are the coefficients α_{ik}. Typically, M equals the number of elements in the system, although in some cases it may be smaller. Multiplying the transport equations (Eq. 9) through by α_{ik} and summing over i gives

$$\sum_{i=1}^{N} \alpha_{ik}\left(\frac{\partial (C_i + C_i^a)}{\partial t} + \nabla\cdot j_i = R_i\right), \quad \forall\, k = 1,\cdots, M \tag{11}$$

but since the total mass of each element is conserved

$$\sum_{i=1}^{N} \alpha_{ik}R_i = 0 \tag{12}$$

Then, using Eq. 10 we may write

$$\frac{\partial T_k}{\partial t} + \sum_{i=1}^{N} \alpha_{ik}\nabla\cdot j_i = 0, \quad \forall\, k = 1,\cdots, M \tag{13}$$

The set of Eqs. 13 avoids the stiffness problem since only the time scales of the transport processes need be resolved.

This approach has been successfully applied in a number of cases to model the transport of reacting multicomponent systems in groundwater (Walsh et al., 1984; Cederberg et al., 1985). In these applications, however, it is assumed that the dispersion coefficients of the species associated with a given conserved quantity are equal. The equivalent constraint is not

imposed here since the transport of the conserved quantities is determined from the contribution of each individual species flux.

Once the values of the conserved quantities T_k are known at a given time from integrating Eq. 13, the individual species concentrations in the bulk solution and sorbed in the solid are determined by solving the algebraic relations for chemical and sorption equilibrium. For a chemical system with N chemical species and M conserved quantities, a system of $2N$ equations with $2N$ unknowns is set up as follows:

2N Unknowns. Concentrations of the individual species in solution and adsorbed in the soil $\{C_1,\cdots,C_N\}$, $\{C_1^a,\cdots,C_N^a\}$.

2N Equations.

- M conservation equations (Eq. 10) with the value of the conserved quantities T_k determined from the transport equations (Eq. 13).
- N sorption isotherms

$$C_i^a = f_i(C_1,\cdots,C_N) \tag{14}$$

- and $N-M$ mass action equations of the form

$$K_j = \prod_{i=1}^{N} (C_i)^{\nu_{ij}} \tag{15}$$

with the concentrations here expressed in molarity. K_j is the equilibrium constant and ν_{ij} the stoichiometric coefficient for species i in the jth chemical equation (with negative value for the reactants). For example, in the reaction

$$H_2CO_3 \rightleftharpoons H^+ + HCO_3^-$$

the stoichiometric coefficients are -1 for H_2CO_3, 1 for H^+, and 1 for HCO_3^-.

The solution to the system of algebraic equations defined by Eqs. 10, 14 and 15 is the last step in the determination of the individual species concentrations. Note that in this approach, the chemical equilibrium calculation can be handled as a separate module or functional unit within the main electroremediation model. Furthermore, the conserved quantities T_k are typically the input data required by commercially available chemical equilibrium programs. As a result, different chemical systems can be described with minimum change to the numerical code, customized models of the chemical system can be verified by comparing them with standard equilibrium programs, and even commercial equilibrium programs can be used as part of the electroremediation model.

It is not always possible to assume equilibrium for all of the chemical reactions. For example, slow dissolution or precipitation reactions may not reach equilibrium in the time scales of the transport processes (Table 1). With some modifications, however, the conserved quantities approach can still be applied. The first step is to classify the reactions into two groups: those whose characteristic times are much smaller than the transport times, which are assumed to be fast; and those with characteristic times of the same order as the transport times, which are assumed to be slow. In the transport time scales, a pseudo-equilibrium state (Morel and Hering, 1993) is then assumed to exist, where the total amount of reactants and products available for fast chemical transformations is controlled by the transport and slow chemical reactions. The corresponding transport equations will contain only the generation terms associated with the slow reactions. These equations will not be numerically stiff since, by definition, the characteristic times of the slow reactions and transport processes are of the same order.

Charge balance and electroneutrality

Assuming that the soil is neutral prior to contact with the pore liquid, the total charge density in the system T_0 in C/m^3 can be obtained from the concentrations of species in solution and in the solid phase:

$$T_0 = F \sum_{i=1}^{N} z_i(C_i + C_i^a) \tag{16}$$

Here, the solid phase is taken to include the thin double layer, whence since the net charge on the soil and in the double layer must be zero

$$F \sum_{i=1}^{N} z_i C_i^a = 0 \tag{17}$$

Then, from Eq. 17 and the electroneutrality condition

$$\sum_{i=1}^{N} z_i C_i = 0 \tag{18}$$

we see from Eq. 16 that

$$T_0 = 0 \tag{19}$$

Using Eq. 18 or 19, one of the transport equations (Eq. 13) can be replaced by an algebraic equation. In practice, eliminating the transport equation that involves the fastest moving species (usually the hydrogen ions) is advantageous in the numerical implementation of the model since it relaxes the constraints on the mesh resolution and time-step size for numerical stability. Also, note that Eq. 17 imposes a constraint on the sorption isotherms (Eq. 14), so only $N-1$ independent isotherms are needed.

Electrostatic potential and pressure distributions

The electrostatic potential distribution at any given time is determined by applying conservation of charge. Assuming that the soil matrix is conducting, the total current density $\boldsymbol{i}$ (A/m^2) will include the contributions from ion transport in the liquid phase, and conduction in the solid given by Ohm's Law:

$$\boldsymbol{i} = F \sum_{i=1}^{N} z_i \boldsymbol{j}_i - \sigma_s \nabla\phi, \tag{20}$$

where σ_s in S/m is the apparent electrical conductivity of the soil.

Taking a charge balance in an infinitesimal control volume of the porous medium gives

$$\frac{\partial}{\partial t}\left(F\sum_{i=1}^{N} z_i(C_i + C_i^a)\right) + \nabla\cdot\boldsymbol{i} = F\sum_{i=1}^{N} z_i R_i = 0 \quad (21)$$

and from the definition Eq. 16,

$$\frac{\partial T_0}{\partial t} + \nabla\cdot\boldsymbol{i} = 0 \quad (22)$$

This equation shows that since there is no accumulation of charge (Eq. 19),

$$\nabla\cdot\boldsymbol{i} = 0 \quad (23)$$

Moreover, substitution of Eq. 20 into Eq. 23 shows the fluxes of the individual species are not independent, but are constrained by

$$\nabla\cdot\left(F\sum_{i=1}^{N} z_i\boldsymbol{j}_i\right) = \nabla\cdot(\sigma_s\nabla\phi) \quad (24)$$

Substituting the expressions for the species fluxes (Eq. 5) into Eq. 24, neglecting the contribution of convection to the current density, and reordering terms

$$\nabla\cdot\left(F\sum_{i=1}^{N} z_i\boldsymbol{u}_{ei}C_i\right) - \nabla\cdot(\sigma_s\nabla\phi) = \nabla\cdot\left(F\sum_{i=1}^{N} z_i\frac{D_i}{\tau^2}\nabla C_i\right) \quad (25)$$

Using the definition of the electromigration velocities $\boldsymbol{u}_{ei}$ (Eq. 3), Eq. 25 may be written

$$-\nabla\cdot(\sigma\nabla\phi) = \nabla\cdot\left(F\sum_{i=1}^{N} z_i\frac{D_i}{\tau^2}\nabla C_i\right) \quad (26)$$

where σ is the electrical conductivity of the medium, which is defined by

$$\sigma = \frac{F^2}{\tau^2}\sum_{i=1}^{N} z_i^2 v_i C_i + \sigma_s \quad (27)$$

Thus, at any time, the electrostatic potential can be determined from the individual species concentration distributions by solving Eq. 26 subject to appropriate boundary conditions.

In the present work, the porous medium is assumed to be saturated and incompressible, approximations which can be relaxed at the expense of increased complexity. In a saturated incompressible porous medium, the pressure distribution is determined by a procedure analogous to that used to determine the electrostatic potential. Applying mass conservation to the pore liquid,

$$\nabla\cdot\boldsymbol{u}_c = 0 \quad (28)$$

and substituting the expressions for the electroosmotic and hydraulic pressure contributions to the bulk liquid velocity, gives

$$-\nabla\cdot(k_h\nabla p) = \nabla\cdot(k_e\nabla\phi) \quad (29)$$

This equation is used to determine the pressure distribution once the electrostatic potential distribution is known.

Boundary conditions

To complete the formulation we next specify the boundary conditions. As can be seen in Figure 1, the boundary of the domain is defined by the union of the external boundary and the walls of the electrode reservoirs. The external boundary is assumed to be formed by impermeable, nonreacting, nonconducting walls, so no-flux boundary conditions are imposed. The interior of the electrode reservoirs is not included in the computational domain to avoid the uncertain nature of the flow inside the reservoir and the complicated phenomena occurring near the active electrodes. Thus, the concentrations of the chemical species, the potential and the pressure at the porous walls separating the soil, and the liquid inside the reservoir boundaries need to be specified.

In terms of the flow rate at each well Q_w in m^3/s, two classes of electrodes are defined: *sink electrodes* are those where the pore liquid flows from the soil into the electrode reservoir ($Q_w > 0$); and *source electrodes* are those where the liquid flows from the electrode reservoir into the soil ($Q_w \le 0$) (Probstein et al., 1991). Well-mixed conditions are assumed in the reservoirs and the concentration boundary conditions are derived by applying mass conservation for each chemical species inside the electrode reservoirs.

The mass balances are defined here for two operating modes: *electrode draining*, where the pore liquid entering the sink electrodes overflows to effuent collectors with the liquid flowing out of the source electrodes replaced by a purge solution; and *electrode washing*, where an external solution is circulated through the electrode reservoirs, maintaining a constant volume of liquid. The wash solution flow rate is considered high enough to maintain an essentially neutral pH in the electrode well.

For the case of electrode draining, by applying mass conservation and the definition of a conserved quantity (Eq. 10), the differential equation describing the conditions at the boundary of reservoir w can be shown to take the form

$$V_w\frac{d(T_k^{\text{well}})_w}{dt} = \sum_{i=1}^{N}\alpha_{ik}(\phi_{A_w}\boldsymbol{j}_i\cdot\hat{\boldsymbol{n}}dA) - Q_w(T_k^{io})_w + V_w\sum_{i=1}^{N}\alpha_{ik}(R_i^e)_w \quad (30)$$

where $(T_k^{\text{well}})_w$ in mol/m^3 and $(T_k^{io})_w$ are, respectively, the concentrations of the conserved quantity k in the electrode well and in the solution going in and out of the system (purge solution or effuent), A_w in m^2 is the area available for mass transfer, V_w in m^3 the volume of the reservoir, and $(R_i^e)_w$ in $mol/(m^3\cdot s)$ is the net volumetric rate of production of species i due to electrochemical reactions. The lefthand side of Eq. 30 is the rate of change of the total mass of conserved quantity k in the electrode reservoir w. The first term on the righthand side is the net flux of the conserved quantity into the reservoir based on the flux of its constituents. The second term is the flux leaving the system in the effluent or being incorporated into the system in the purge solution, and the last term corresponds to the electrochemical generation.

Assuming that the electrochemical reactions are at steady state, the net rate of species production due to these reactions is calculated from Faraday's law

$$(R_i^e)_w = \frac{(\gamma_{ie})_w}{V_w} \oint_{A_w} \frac{(\hat{n}\cdot i)}{F} dA \tag{31}$$

where $(\gamma_{ie})_w$ is the number of moles of species i produced per mole of electrons captured or released in the electrochemical reactions occurring at electrode w. That is, $1/z_i$ for the reacting species and 0 for the nonreacting species. For example, in the water electrolysis reactions

$$2H_2O + 2e^- \rightarrow 2OH^- + H_2(g) \qquad \text{(cathode)}$$

$$2H_2O \rightarrow 4H^+ + O_2(g) + 4e^- \qquad \text{(anode)}$$

the stoichiometric coefficients $(\gamma_{ie})_w$ are 1 for H^+ and 0 for OH^- at the anodes, and 0 for H^+ and 1 for OH^- at the cathodes.

Note that since there is current continuity, the total current through the reservoir boundary equals the total current through the active electrode. Therefore, the generation rate given by Eq. 31 is the same as would be obtained by applying Faraday's law at the active electrode. Similar forms for the equations describing the reservoir boundary conditions are obtained for the case of electrode washing. A more detailed discussion of the boundary conditions may be found in Jacobs (1995).

Solution procedure

Based on the elements of the model described, the procedure to advance the solution from an initially prescribed or determined state at time t (spatial distribution of the individual species concentrations $\{C_1,\cdots,C_N\}^t$, $\{C_1^a,\cdots,C_N^a\}^t$) to a subsequent time step may be summarized as follows:

(1) Calculate the value of the variable properties that depend on the ionic environment or are space dependent (such as zeta potential, hydraulic permeability, and species diffusivities).

(2) Solve the current continuity equation (Eq. 23: $\nabla\cdot\boldsymbol{i} = 0$), subject to appropriate boundary conditions, to determine the spatial distribution of the electrostatic potential ϕ.

(3) Solve the mass conservation equation for the pore liquid (Eq. 28: $\nabla\cdot\boldsymbol{u}_c = 0$), subject to appropriate boundary conditions, to determine the pressure distribution p.

(4) Calculate the species fluxes $\boldsymbol{j}_i$ (Eq. 5) from the known concentration distributions and the electrostatic potential and pressure distributions determined in steps 2 and 3.

(5) Integrate the ordinary differential equations describing the boundary conditions (Eq. 30) to find the values of the conserved quantities in the electrode reservoirs $(T_k^{\text{well}})_w$ at the new time $t + \Delta t$.

(6) Integrate the transport equations (Eq. 13), subject to the specified boundary conditions (step 5), to find the spatial distribution of the conserved quantities T_k at the new time $t + \Delta t$.

(7) Solve for chemical and adsorption equilibrium (Eqs. 10, 14 and 15) to find the spatial distribution of the individual species $\{C_1,\cdots,C_N\}$, $\{C_1^a,\cdots,C_N^a\}$ at the new time $t + \Delta t$.

Numerical Code

Difficulties in the numerical solution of the electroremediation model set out arose, not only because of the interaction between the transport of mass and charge and because the solution involves a strongly nonlinear system of partial differential and algebraic equations, but more importantly because of the development of thin boundary layers, high localized electric fields, and kinematic shocks in the solution. These latter factors result in severe constraints on the mesh resolution and the time-step size for numerical stability.

To overcome these difficulties, several integration schemes, such as the fluctuation splitting schemes used in gas dynamics (Deconinck et al., 1994), the Petrov-Galerkin finite-element methods for convection-dominated flows (Hughes, 1989), and the Galerkin method with added isotropic or streamwise diffusivity (Ames, 1992) were investigated.

The computational domain was discretized with linear triangular elements using an automatic unstructured mesh generator (Hecht and Saltel, 1990). The mesh generation algorithm is described by Hecht and Saltel (1991). Linear basis functions were chosen so that the fluctuation splitting schemes, which assume linear variation of all variables within each triangle, may be used. These methods showed great potential for application in the electroremediation model, because they were developed to solve the Euler equations for inviscid compressible flows, and in these flows the transport of mass, momentum, and energy is dominated by advection in the same way that the transport of mass is dominated by convection and migration in electroremediation.

The elliptic equations used to determine the electrostatic potential and pressure distributions (Eqs. 26 and 29) were discretized using the Galerkin finite-element formulation. This resulted in a set of discrete equations.

$$\boldsymbol{A}\tilde{\boldsymbol{u}} = \boldsymbol{f} \tag{32}$$

where the system matrix $\boldsymbol{A}$ is symmetric, positive definite, and sparse, $\tilde{\boldsymbol{u}}$ is a vector of unknowns formed by the electroostatic potential or pressure at each node, and $\boldsymbol{f}$ is a force vector derived by multiplying the righthand side of Eq. 26 and 29 times trial functions and integrating over the computational domain.

It was found that the Galerkin finite-element formulation provided the best platform for the discretization of the differential equations of the problem. A critical factor affecting the fluctuation-splitting schemes and the other upwind techniques was that Eq. 32, used to determine the electrostatic potential distribution, could not be recovered by a linear combination of the discretized transport equations. As a result, these methods could not effectively capture the coupling between the transport of mass and charge and failed to maintain electroneutrality in the solution.

The use of explicit vs. implicit time integration was evaluated with the aim of reducing the overall execution time of the code. Due to the coupling between the transport, chemical equilibrium, and electrostatic potential calculation steps, the computational load associated with implicit schemes was high and resulted in lower overall execution speed than that achieved using explicit schemes.

Due to the convergence and numerical stability requirements of the Galerkin formulation, it was necessary to intro-

duce an artificial diffusivity in order to approximate the solution for cases with high migration or convection velocities. The artificial diffusivity was added to the diffusion coefficients used in the transport equations so that the maximum grid Peclet number over the computational domain for the species included in the transport equations was less than two. It has been shown (Ames, 1992) that for the linearized, 1-D version of the convection diffusion equation, this criterion is used in determining whether oscillation or wiggles will appear in the steady-state solution. Here, it was applied to the transient case with the idea that the mesh at any time during the simulation had to be fine enough to represent the steady-state solution. Also, in the nonlinear, 2-D case considered, the criterion was applied locally in time and space.

Since the main features of the solution are dominated by convection and migration, this had little effect on the global concentration distributions predicted by the model. It was found, however, that care must be taken in interpreting the model predicitions near the electrode reservoirs since some variables, which depend on an estimate of the species fluxes at the boundary, are sensitive to the mesh resolution. When required, the quality of the local solution can be improved by reducing the local mesh spacing. For additional details on the numerical solution see Jacobs (1995).

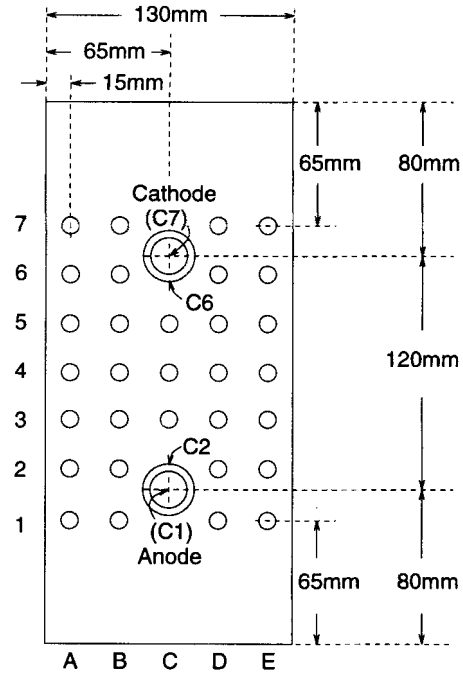

Figure 3. Identification and location of passive electrodes in the test cell.

Experimental Measurements

An experiment on the removal of phenol from kaolin clay was carried out in a 0.28-m-long, 0.13-m-wide and 0.07-m-deep closed rectangular acrylic cell containing a single anode/cathode pair separated by about 0.12 m along the centerline (Figure 2). The electrode reservoirs were made of plastic tubes about 0.03 m in diameter with a perforated section extending into the soil section of the test cell. Both electrode wells were open at the top to vent the electrolysis gases and the graphite rods used as active electrodes were submerged in the liquid filling the wells. An array of passive electrodes made of 1/8-in. (3.2-mm) stainless steel tube extended about 0.03 m from the top section of the cell in the area between the electrodes to measure the electrostatic potential distribution during the experiment (Figure 3). Since the active electrodes extended vertically throughout the depth of the test module, and the soil sample was isolated from the environment by nonconducting, impermeable walls at both the top and bottom of the test section, the conditions in the 3-D geometry of the experiment were considered to be well represented by a 2-D model. That is, conditions in horizontal planes were approximately uniform with depth.

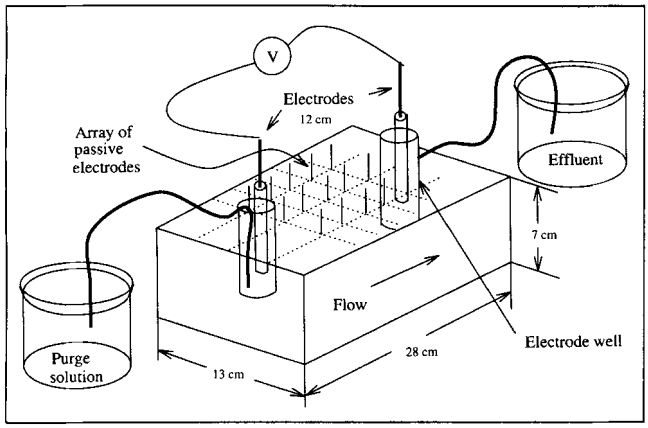

Figure 2. Experimental setup.

The test cell was filled with the contaminated sample prepared by mixing dry kaolin clay (supplied by Albion Kaolin Co., Hephzibah, GA) with a 4.782-mM ($\approx$ 450-ppm) solution of phenol in distilled water in a weight proportion of 38% liquid and 62% clay. The electrode wells were filled with tap water, and a voltage of 40 V was applied to the active electrodes and maintained for about 33 days. A 10-mM NaOH purge solution was introduced at the source electrode (anode) well while the effluent spillover in the sink electrode (cathode) reservoir was collected for analysis.

At the conclusion of the experiment, the sample was split in 35 sections arranged in a rectangular array over the test module (Figure 2). The pore liquid was pressed out and analyzed for phenol content and pH. These measurements were taken to be representative of the mean conditions over the depth of the cell. Very high contaminant removal was achieved in most of the cell with the largest remaining concentrations being less than 12% of the initial concentration and the average level of removal being about 96%. The pH measured at the end of the experiment was relatively uniform at about 5.5, which suggests that the buffering capacity of the system was large compared with the amount of hydrogen and hydroxyl ions produced at the electrodes.

The electroosmotic flow rate observed throughout the experiment was quite steady, with small variations around an average value of 201.5 mL/d. The electrostatic potential distribution was smooth with moderate changes near the cathode. The concentration of phenol in the effluent increased to

about 3.5 mol/m^3 during the first day and then decayed more or less exponentially with the amount of effluent displaced.

The amount of contaminant removed, which was calculated by multiplying the concentration in the effluent times the volume of the effluent displaced, was about 80% of the initial value, which indicates an error of about 16% in the mass balance when compared with the amount of phenol measured at the end of the experiment. This difference is attributed to evaporation and handling losses as well as chemical degradation of phenol into non-HPLC-detectable forms that took place in both the effluent and soil samples during the period prior to analysis.

Numerical Simulations

Three different cases of increasing complexity were considered to describe the phenol experiments. The first representation was a neutral species description which only included the role of convection and diffusion, the second added electromigration and chemical transformations in the pore liquid, while the third representation also incorporated the soil acid/base chemistry. The comparison of the model predictions for these three cases with the experimental data provided a striking illustration of the role of the different transport mechanisms and chemical processes on the removal of phenol from kaolin clay in the experiment.

In the neutral species simulation, no charged species were assumed to exist in the system, and all chemical transformation and sorption processes were neglected. The electrostatic potential and pressure distributions were determined assuming uniform electrical conductivity and uniform hydraulic and electroosmotic permeabilities. These simplifying assumptions were made based on the observation of a relatively uniform pH of about 5.5 at the conclusion of the experiment. Considering that the hydrogen ions carry most of the current, and that the zeta potential depends strongly on the pH of the pore solution, it was inferred that this uniform pH probably resulted in uniform electrical conductivity and electroosmotic permeability. In addition, since the pH in the cell remained well below the pKa of phenol, the contaminant was taken to be neutral in most of the domain. This simulation indicated the role of electroosmosis in the contaminant removal experiment considered.

A summary of the parameters and initial conditions used in the neutral species simulation is given in Table 2. The potentials at walls of the electrode reservoirs were derived from measurements at the active electrodes and the neighboring passive electrodes. The tortuosity was evaluated independently from 1-D conductivity measurements as explained in Shapiro (1990), the hydraulic permeability was determined from permeability measurements, and the porosity was calculated from the mass fraction and the densities of the liquid and the dry solid. The zeta potential was selected to fit the observed flow rate.

The calculated concentration distributions at several times during the experiment are presented in Figure 4. The advancement of the clean front due to electroosmosis can be seen as the purge solution is introduced into the system, and the concentration near the corners of the test module is seen to decrease at a much slower rate, because of the spatial decay of the electric field, than the concentration in the area between the electrodes where purging was most effective.

Table 2. Parameters and Initial Conditions in the Neutral Species Simulation

Parameter	Values
Cell dimensions	$0.28\times0.13\times0.0683$ m
Distance between active electrodes	0.12 m
Diameter of electrode wells	0.0283 m
Pressure at electrode wells, $\{p_1, p_2\}$	10^5 Pa
Potential at the anode well, ϕ_1	35.0 V
Potential at the cathode well, ϕ_2	6.2 V
Porosity, n	0.6144
Tortuosity, τ	1.25
Hydraulic permeability, k'_h	10^{-15} m^2
Zeta potential, ζ	-5.4×10^{-3} V
Pore liquid electrical permittivity, ϵ	7.0×10^{-10} F/m
Pore liquid viscosity, μ	10^{-3} Pa·s
Effective hydraulic permeability, k_h	10^{-10} m^2/(Pa·s)
Effective electroosmotic permeability, k_e	-2.4×10^{-9} m^2(V·s)
Soil conductivity, σ_s	0.001 S/m
Initial concentration in test cell	4.782 mol/m^3
Initial concentration in wells	0 mol/m^3
Diffusion coefficient of phenol, D	10^{-9} m^2/s

The concentration of phenol in the effluent calculated using the neutral species model is compared with the measured values in Figure 5. The model overestimates the concentration of phenol in the effluent during the first five days of experiment (≈ 0.4 pore volumes). However, the general agreement of the model predictions with the experimental data is quite good. This close agreement between the model and the experimental data confirms that the phenol system generally behaves as a neutral species system under the conditions of the experiment.

In the second simulation, the acid/base reactions of water and phenol in the pore liquid and the water electrolysis reactions at the electrodes were included. The model also described the coupled transport of mass and charge due to convection, electromigration, and diffusion, and considered the role of the ionic environment and the contribution of diffusion to the current density when determining the electrostatic potential distribution. The effect of adsorption was not in-

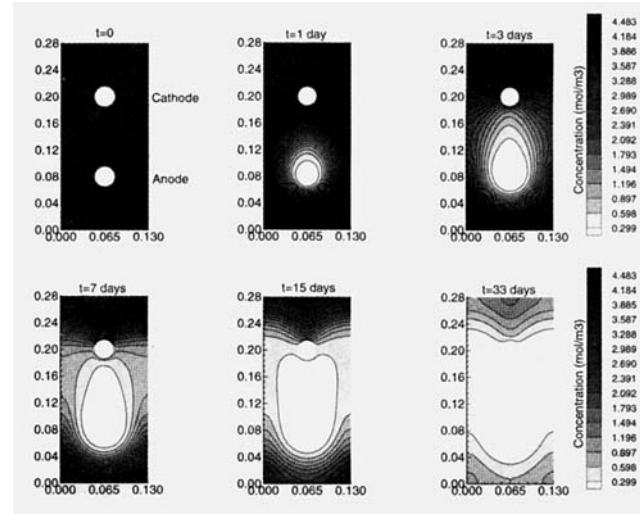

Figure 4. Calculated concentration distributions at $t = 0$, 1, 3, 7, 15 and 33 d using the neutral species model.

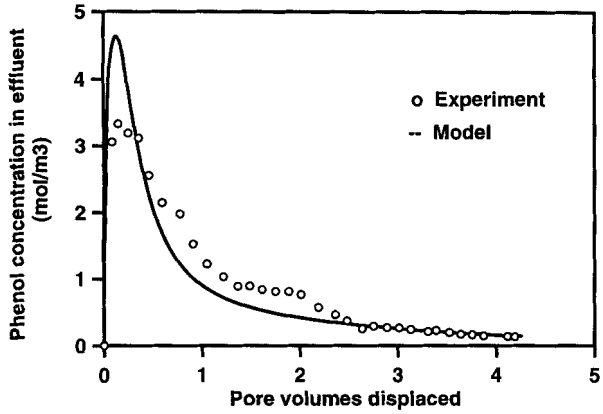

Figure 5. Measured concentration of phenol in the effluent vs. calculated values using the neutral species model.

cluded since laboratory measurements indicated a linear adsorption isotherm with slope $K_d = 0.075$ (Shapiro, 1990). This isotherm corresponds to a retardation factor of 1.075 which does not significantly affect the phenol concentration distributions or the time scale for removal.

Based on the species in Table 3, the system of equations in this case has six unknowns ($\{C_1, \cdots, C_6\}$) and six equations setup as follows:

- *Four Conservation Equations*

$$T_0 = C_1 - C_2 - C_4 + C_5 - C_6 \qquad T_1 = C_3 + C_4$$
$$T_2 = C_5 \qquad T_3 = C_6 \tag{33}$$

with $T_0 = 0$ and $\{T_1, T_2, T_3\}$ determined from the transport equations.

- *Two Mass Action Equations*

$$K_1 = C_1 C_2, \qquad K_2 = C_1 C_4 / C_3 \tag{34}$$

Note that the system has five elements, H, O, C, Na, and Cl, and seven species, including H_2O. The rank of the formula matrix for this system is five, so the number of conserved quantities should be five, yet only four conserved quantities are shown in Table 3. The fifth component, not shown in Table 3, is water. Taking H_2O as a component avoids the appearance of the water concentration (approximately 55.4 M) in any of the conservation equations except that for water itself. This minimizes the occurrence of round-off errors in the solution. Since the activity of water is 1 in the mass action equations and its concentration does not appear in the conservation equations of the components, there is no need to track the total amount of water in the system. Therefore, only four conserved quantities are used in the simulation. This approach is used when modeling electromediation in aqueous systems.

Table 3. Nomenclature Used in Weak Acid Description of Phenol System

Species	Conc.	Conserved Quantity	Symbol
H^+	C_1	Charge	T_0
OH^-	C_2	Total Phenol	T_1
C_6H_5OH	C_3	Na	T_2
$C_6H_5O^-$	C_4	Cl	T_3
Na^+	C_5		
Cl^-	C_6		

Table 4. Mobility and Diffusion Coefficients Used in Weak Acid Description of Phenol System

	Species	Mobility mmol/(N·s)	Diff. Coeff. m^2/s
1	H^+	3.756×10^{-12}	9.311×10^{-9}
2	OH^-	2.127×10^{-12}	5.273×10^{-9}
3	C_6H_5OH	4.036×10^{-13}	1.000×10^{-9}
4	$C_6H_5O^-$	4.395×10^{-13}	1.089×10^{-9}
5	Na^+	5.379×10^{-13}	1.334×10^{-9}
6	Cl^-	8.197×10^{-13}	2.032×10^{-9}

The values of the relevant parameters used in this simulation were the same as those in Table 2. The mobilities and diffusion coefficients of the chemical species are given in Table 4. These values are adapted from Vaný sek (1993). The initial conditions in the cell were $T_1 = 4.782$ mol/m^3, $T_2 = T_3 = 0.1$ mol/m^3, and in the electrode reservoirs $T_1 = 0$, $T_2 = T_3 = 1$ mol/m^3.

The electrolysis reactions at the electrodes together with the transport of the background ions Na^+ and Cl^- play a major role in the response of the system. As time progresses, the sodium ions accumulate in and near the cathode reservoir while the negatively charged chloride ions migrate toward the anode and accumulate in the reservoir there. This accumulation takes place because the migration velocities of the sodium and chloride ions are initially about one order of magnitude larger than the bulk liquid velocity. At the same time, the hydroxyl ions produced at the cathode and the hydrogen ions produced at the anode migrate toward the center and meet at a region intermediate between the electrodes to form water.

Near the cathode the excess charge of the sodium ions over the chloride ions is balanced mainly by the hydroxyl ions and in a lower proportion by the phenolate ions, while near the anode the excess charge of the chloride over the sodium ions is balanced by hydrogen ions. Recall that the transport of mass and the transport of charge are coupled through the condition of electroneutrality, so that at any point in space the concentrations resulting from the transport are such as to maintain a neutral solution.

The transport of ions and the chemical transformation of hydrogen and hydroxyl ions into water result in the development of a pH shock in the interior of the cell. This shock can be seen in Figure 6, which shows the calculated pH distribution at different times during the simulation.

The development of the pH shock is paralleled by the development of a high localized electric field because of the sharp change in electrical conductivity. In addition, the pH has a large effect on the transport of phenol in the system. At the high pH side of the jump the pH is larger than the pKa of phenol (about 9.9), so that a significant fraction of the contaminant is dissociated into the negatively charged phenolate ion and migrates from the cathode to the anode. On the other hand, at the low pH side of the jump the pH is much smaller than the pKa and virtually all the phenol is neutral and moves

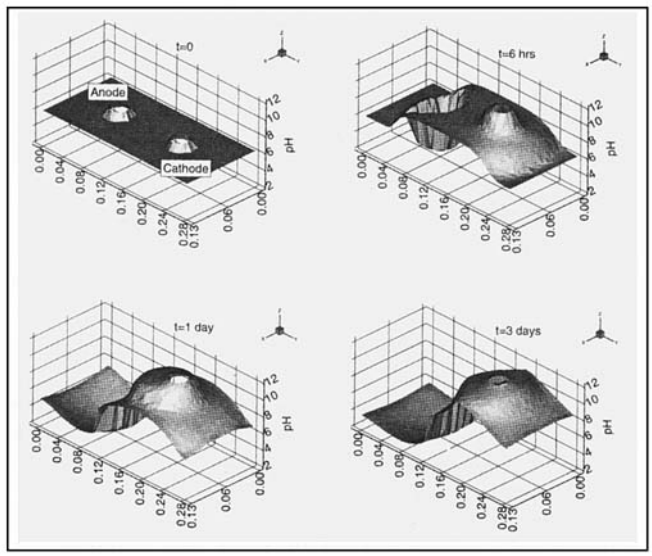

Figure 6. Calculated pH distribution at $t = 0$, 6 h, 1 d, and 3 d using the weak acid model.

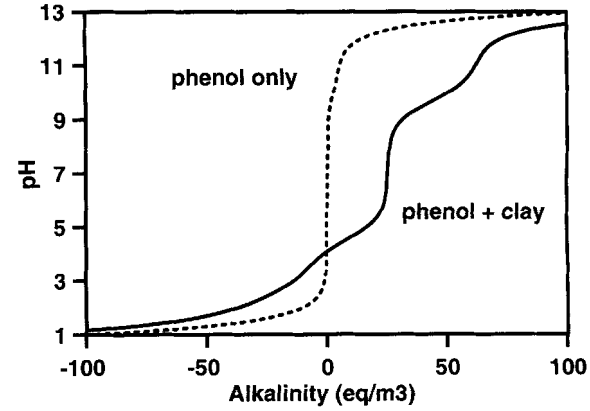

Figure 7. Calculated equilibrium pH as a function of alkalinity.

For a 4.78-mM phenol solution alone (· · · · · ·) vs. a mixture of kaolin clay and a 4.78-mM phenol solution in a 1.5:1 solid to liquid mass ratio (—).

with the pore liquid from the anode to the cathode. This effect prevents the phenol from being removed from the cell but results in the accumulation of the contaminant in a narrow band of the soil at the location of the pH jump.

This focusing effect was described in the context of 1-D metal removal experiments by Probstein and Hicks (1993). Details of the experimental procedure and additional analysis of the phenomenon were presented by Hicks and Tondorf (1994), while a successful simulation through a mathematical model was given by Jacobs et al. (1994). In the metal removal case, the focusing effect involved metal species migrating in converging directions at each side of the pH jump and precipitating at the point of minimum solubility. In the case considered here, the phenomenon is shown to occur without the participation of precipitation reactions.

The experimental data, however, did not show the development of the pH jump predicted by the model but rather a uniform pH distribution. Moreover, the observed potential distribution was smooth, without the sudden changes observed in the model calculations. This discrepancy between the model predictions and the experimental data suggested that the buffer capacity of the system was not small compared with the acid and base generated at the electrodes, and that an important element was left out in the chemical description of the phenol system.

In the last simulation, the description of the phenol system was upgraded by considering the acid/base chemistry of the clay. The chemical action of the clay was represented in terms of a combination of immobile weak acids and bases. The total amount of these compounds, and the equilibrium constants associated with their reactions were selected to fit measured titration data. This soil chemistry model was not intended to provide a detailed representation of the clay surface chemistry, rather it merely aimed at capturing the effect of the clay on the acid/base chemistry of the system. For a detailed description of kaolinite chemistry see Grim (1968). Note, however, that the ion-exchange capacity and the titration data observed in any particular case depends heavily on factors such as the presence of impurities, the particle-size distribution, and the degree of crystallinity, so the use of direct measurements on the soil of interest cannot generally be avoided.

The role of the clay on the pH response of the system is clearly illustrated in Figure 7 which shows calculated titrations for a 4.78 mM solution of phenol and no clay (dotted line), and a mixture of clay and the same phenol solution (solid line). The departure of the mixture's behavior from that of the solution alone is clearly seen.

When the buffering effects of the soil are included in the simulation, no pH jump develops inside the cell. Instead, the pH distribution remains almost uniform over the cell with changes occurring only in the electrode reservoirs, as observed in the experiment. This pH distribution translates into a relatively uniform electrical conductivity in the interior of the cell and a much higher conductivity at the electrode reservoirs, especially at the cathode. As a consequence, the electric field strength is very low and the relative contribution of convection to the species flux is important in the proximity of the electrode reservoirs.

Figure 8 shows the calculated phenol concentration distributions obtained for this case. The distributions are seen to be very similar to the ones shown in Figure 4 for the neutral species simulation. In most of the test module the pH is well below the pKa of phenol, so that the contaminant remains in its neutral form and moves with the pore liquid.

As the pH increases in the cathode reservoir, the phenol transforms into the negatively charged phenolate form and migrates upstream toward the anode. It soon reaches the low pH region of the soil, transforms back into the neutral form, and resumes its travel toward the cathode. This process results in the rejection and subsequent accumulation of phenol at the interface between the soil and the electrode well where the pH change occurred. This accumulation can be seen in Figure 8 in the concentration distributions at $t = 6$ h, 1 day, and 3 days. At the same time, the accumulation of sodium and hydroxyl ions in the cathode reservoir results in the increase of the electrical conductivity and the reduction of the local electric field strength, so that as time progresses con-

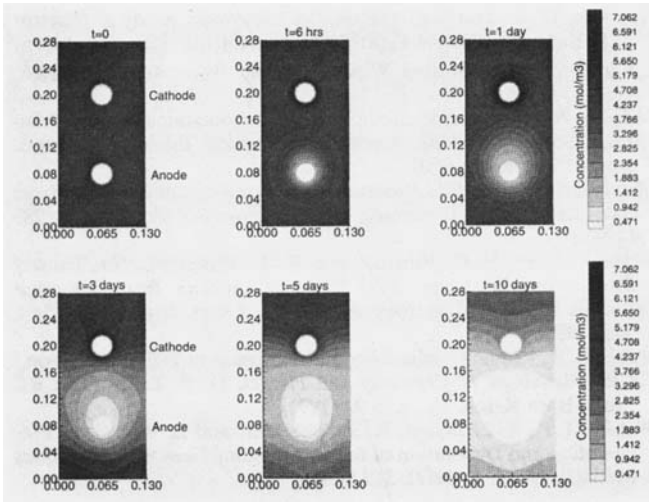

Figure 8. Calculated phenol concentration distributions at different times during the 10-d simulation period.

Obtained using the weak acid + soil chemistry description of the system.

vection becomes more important near the cathode and the focusing effect weakens.

Eventually, a quasi-equilibrium condition is reached in which the upstream migrational flux of the phenolate ions balances the net favorable diffusional flux of phenol into the reservoir. At this point, accumulation of phenol stops and the convectional flux at the low pH side of the region appears to go through the pH jump unaffected. At later times, convection becomes dominant near the cathode reservoir and the neutral species behavior is recovered. This transition can be observed in the predicted concentration distributions at $t = 3$, 5 and 10 days. This behavior described explains the reason for the close agreement between the model predictions for the neutral species simulation and the observed phenol concentrations in the effluent.

For the conditions considered, the last simulation predicts the correct pattern of behavior of the phenol concentration in the effluent (a sudden increase, short plateau, and then slow decrease, see Figure 5), but significantly underestimates the absolute value of the effluent phenol concentration. This is a consequence of the introduction of artificial diffusivity as part of the solution method and the use of linear elements. These factors result in inaccurate descriptions of the concentration gradients at the boundary. This has little effect on the solution outside of the boundary layer, where transport is dominated by convection and migration, but has a significant effect on the local solution.

Conclusions

A principal benefit of the conserved quantities approach and of the explicit time integration of the transport equations is the effective decoupling of the transport and chemical equilibrium calculations. As a result, the chemical and sorption equilibrium calculations can be handled as a separate module or functional unit within the main electroremediation program. This facilitates the description of different chemical systems and enables the use of commercial equilibrium programs as part of the electroremediation code.

The Galerkin finite-element formulation with added isotropic diffusivity provided the best platform for the discretization of the differential equations of the problem. A key property of the approach is that the set of discrete equations used to determine the electrostatic potential distribution can be obtained from the discretized transport equations. This property is not common to all discretization schemes, but is crucial to maintain electroneutrality in the solution.

The significantly different responses predicted by the model for the cases with and without the acid/base chemistry of the soil indicates that the value of the system buffer capacity relative to the expected acid/base generation at the electrodes is a crucial parameter to evaluate when assessing the remediation of a site by electric fields.

Under certain conditions, a focusing effect similar to that described by Probstein and Hicks (1993) for metals removal can occur when removing weak acids (even soluble, weakly dissociated compounds) from soils by electric fields.

The clay acid/base chemistry was the determining factor in the successful removal of phenol in the experiment described. This highlights the important role that the soil chemistry plays in the electroremediation process.

The results from the test cases and the successful explanation of the experimental observations in terms of the modeled transport and chemical processes confirm the theoretical arguments behind the model. Also, the information obtained from the numerical simulations illustrates the usefulness of the model in providing insight into the complicated behaviors in electroremediation.

Acknowledgments

This work was supported in part by the EPA Northeast Hazardous Substance Research Center at New Jersey Institute of Technology, the Office of Technology Development within DOE's Office of Environmental Management under the Contaminant Plume Containment and Remediation Focus Area program, and the Southern California Edison Company.

Literature Cited

Acar, Y. B., and A. N. Alshawabkeh, "Modeling Conduction Phenomena in Soils Under an Electric Current," *Proc. Int. Conf. Soil Mech.*, New Delhi, p. 662 (1994).

Alshawabkeh, A. N., and Y. B. Acar, "Removal of Contaminants from Soils by Electrokinetics: A Theoretical Treatise," *J. Environ. Sci. Health, Part A*, **A27**(7), 1835 (1992).

Ames, W. F., "Numerical Methods for Partial Differential Equations," *Computer Science and Scientific Computing*, 3rd ed., Academic Press, San Diego, CA (1992).

Cederberg, G. A., R. L. Street, and J. O. Leckie, "A Groundwater Mass Transport and Equilibrium Chemistry Model for Multicomponent Systems," *Water Res. Res.*, **21**(8), 1095 (1985).

Deconinck, H., R. Struijs, G. Burgois, and P. L. Roe, "High Resolution Shock Capturing Cell Vertex Advection Schemes on Unstructured Grids," *Lecture Ser. Computational Fluid Dynamics*, von Karman Inst. for Fluid Dynamics (Mar., 1994).

Grim, R. E., *Clay Mineralogy*, 2nd ed., McGraw-Hill, New York (1968).

Hamed, J., Y. B. Acar, and R. J. Gale, "Pb(ii) Removal from Kaolinite Using Electrokinetics," *J. Geotech. Eng.*, **117**(2), 241 (1991).

Hecht, F., and E. Saltel, "Emc2: Editeur de Maillages et de Contours Bidimensionnels, Manuel d'Utilisation," Technical Report 118, INRIA (1990).

Hecht, F., and E. Saltel, "Automatic Mesh Generator with Specified Boundary," *Comp. Methods Appl. Mech. Eng.*, **92**, 269 (1991).
Hicks, R. E., and S. Tondorf, "Electrorestoration of Metal Contaminated Soils," *Environ. Sci. Technol.*, **28**(12), 2203 (1994).
Hughes, T. J. R., "A New Finite Element Formulation for Computational Fluid Dynamics: Viii. The Galerkin/Least-Squares Method for Advective-Diffusive Equations," *Comp. Meth. Mech. Engrg.*, **73**, 173 (1989).
Jacobs, R. A., "Two-Dimensional Modeling of the Removal of Contaminants from Soils by Electric Fields," PhD Diss., Dept. of Mechanical Engineering, Mass. Inst. of Technol. (Apr., 1995).
Jacobs, R. A., M. Z. Sengun, R. E. Hicks, and R. F. Probstein, "Model and Experiments on Soil Remediation by Electric Fields," *J. Environ. Sci. Health, Part A*, **A29**(9), 1933 (1994).
Lageman, R., "Electroreclamation. Applications in the Netherlands," *Environ. Sci. Technol.*, **27**(13), 2648 (1993).
Morel, F. M. M., and J. G. Hering, *Principles and Applications of Aquatic Chemistry*, Wiley, New York (1993).
Probstein, R. F., *Physicochemical Hydrodynamics. An Introduction*, 2nd ed., Wiley, New York (1994).
Probstein, R. F., and R. E. Hicks, "Removal of Contaminants from Soils by Electric Fields," *Sci.*, **260**, 498 (1993).
Probstein, R. F., P. C. Renaud, and A. P. Shapiro, "Electroosmosis Techniques for Removing Materials from Soil," U.S. Patent no. 5,074,986 (Dec., 1991).
Runnells, D. D., and J. L. Larson, "A Laboratory Study of Electromigration as a Possible Field Technique for the Removal of Contaminants from Ground Water," *Ground Water Monitoring Rev.*, **6**(3), 85 (1986).
Shapiro, A. P., "Electroosmotic Purging of Contaminants from Saturated Soils," PhD Diss., Dept. of Mechanical Engineering, Mass. Inst. of Technol. (1990).
Shapiro, A. P., and R. F. Probstein, "Removal of Contaminants from Saturated Clay by Electroosmosis," *Environ. Sci. Technol.*, **27**, 283 (1993).
Shapiro, A. P., P. C. Renaud, and R. F. Probstein, "Preliminary Studies on the Removal of Chemical Species from Saturated Porous Media by Electroosmosis," *Phys. Chem. Hydrody.*, **11**(5/6), 785 (1989).
Vaný́sek, P., "Ionic Conductivity and Diffusion at Infinite Dilution," *CRC Handbook of Chemistry and Physics*, D. R. Lide, ed., CRC Press, Boca Raton, FL, p. 5-90 (1993).
Walsh, M. P., S. L. Bryant, R. S. Schechter, and L. W. Lake, "Precipitation and Dissolution of Solids Attending Flow through Porous Media," *AIChE J.*, **30**(2), 317 (1984).

Manuscript received June 12, 1995, and revision received Oct. 4, 1995.